

Spatially-Resolved Eigenmode Decomposition of Red Blood Cells Membrane Fluctuations Questions the Role of ATP in Flickering

Daniel Boss^{1*}, Annick Hoffmann¹, Benjamin Rappaz¹, Christian Depeursinge², Pierre J. Magistretti^{1,3}, Dimitri Van de Ville^{4,5}, Pierre Marquet^{1,3}

1 Brain Mind Institute, Ecole Polytechnique Fédérale de Lausanne, Lausanne, Vaud, Switzerland, **2** Advanced Photonics Laboratory, Ecole Polytechnique Fédérale de Lausanne, Lausanne, Vaud, Switzerland, **3** Centre de Neurosciences Psychiatriques, Département de psychiatrie DP-CHUV, Prilly-Lausanne, Vaud, Switzerland, **4** Institute of Bioengineering, Ecole Polytechnique Fédérale de Lausanne, Lausanne, Vaud, Switzerland, **5** Department of Radiology and Medical Informatics, University of Geneva, Geneva, Switzerland

Abstract

Red blood cells (RBCs) present unique reversible shape deformability, essential for both function and survival, resulting notably in cell membrane fluctuations (CMF). These CMF have been subject of many studies in order to obtain a better understanding of these remarkable biomechanical membrane properties altered in some pathological states including blood diseases. In particular the discussion over the thermal or metabolic origin of the CMF has led in the past to a large number of investigations and modeling. However, the origin of the CMF is still debated. In this article, we present an analysis of the CMF of RBCs by combining digital holographic microscopy (DHM) with an orthogonal subspace decomposition of the imaging data. These subspace components can be reliably identified and quantified as the eigenmode basis of CMF that minimizes the deformation energy of the RBC structure. By fitting the observed fluctuation modes with a theoretical dynamic model, we find that the CMF are mainly governed by the bending elasticity of the membrane and that shear and tension elasticities have only a marginal influence on the membrane fluctuations of the discocyte RBC. Further, our experiments show that the role of ATP as a driving force of CMF is questionable. ATP, however, seems to be required to maintain the unique biomechanical properties of the RBC membrane that lead to thermally excited CMF.

Citation: Boss D, Hoffmann A, Rappaz B, Depeursinge C, Magistretti PJ, et al. (2012) Spatially-Resolved Eigenmode Decomposition of Red Blood Cells Membrane Fluctuations Questions the Role of ATP in Flickering. PLoS ONE 7(8): e40667. doi:10.1371/journal.pone.0040667

Editor: Laurent Kreplak, Dalhousie University, Canada

Received: January 30, 2012; **Accepted:** June 11, 2012; **Published:** August 10, 2012

Copyright: © 2012 Boss et al. This is an open-access article distributed under the terms of the Creative Commons Attribution License, which permits unrestricted use, distribution, and reproduction in any medium, provided the original author and source are credited.

Funding: Funders are in part the Swiss National Science Foundation, grants #CR32I3132993 and #PP00P2123438, URL: <http://www.snf.ch>; and in part the Swiss Commission for Technology and Innovation, grant #9389.1, URL: <http://www.kti.admin.ch>. The funders had no role in study design, data collection and analysis, decision to publish, or preparation of the manuscript.

Competing Interests: The authors have read the journal's policy and have the following conflicts: C.D., P.J.M. and P.M. are co-founders of LynceeTec SA. This does not alter their adherence to all the PLoS ONE policies on sharing data and materials.

* E-mail: daniel.boss@a3.epfl.ch

Introduction

Throughout their lifespan of about 100–120 days, erythrocytes, while being carried throughout the vascular tree to deliver oxygen from the lungs to the tissues, are squeezed as they pass capillaries often smaller than the cell diameter. This ability can be attributed to the remarkable elastic properties of the membrane structure, which consists of a lipid bilayer that is coupled at specific binding sites to the underlying cytoskeleton. This membrane structure exhibits a high resistance to stretch ensuring that no leakage through the lipid bilayer occurs, whereas its low resistance to bending and shear allows the cell to undergo easily shape changes when passing through small capillaries. As a consequence of these elastic properties, RBCs show spontaneous cell membrane fluctuations (CMF), often named flickering, that can be observed under the microscope. This phenomenon has been the subject of considerable scientific interest in the past. One reason is certainly that CMF provide information on the elastic properties of the RBC membrane structure and might help in the diagnosis or understanding of diseases affecting the RBC. Different views on

RBC flickering have been at the origin of research approaches. Brochard and Lennon [1] were among the first to describe quantitatively CMF characteristics. In their theoretical model of the flickering phenomenon, CMF are explained as thermally excited undulations of the cell membrane that are mainly governed by the bending elasticity of the membrane. Using the theoretical model of Brochard and Lennon, a bending modulus of $\kappa \approx (2-7)e-20$ J was determined in a short wavelength regime where the approximation of a flat membrane is valid [1–3]. Strey et al. [4] estimated the bending and shear modulus of erythrocytes in a long wavelength regime based on an eigenmode decomposition of CMF. Contrary to the Brochard and Lennon approach, their theoretical model accounts for a closed cell surface with non-zero equilibrium curvature. A bending modulus of $\kappa = 4e-19$ J was measured in this long wavelength regime. A common result in the above mentioned reports is that shear deformation energy in flickering is negligible; i.e., the shear elasticity of the cytoskeleton is not sensed by the membrane flickering motions in the discocyte RBC. More refined elastic theories that take into account the bilayer-cytoskeleton interactions during flickering were proposed

recently [5,6]. It is noteworthy that the above mentioned estimates of the elastic properties rely on the hypothesis that the driving force of fluctuations is purely thermal. Other authors, however, observed a CMF decrease upon ATP depletion, supporting the view that CMF have also a metabolic origin [7–10]. Levin et al. [7] suggested that an ATP dependent mechano-chemical dynamic assembly of the cytoskeleton could enhance CMF. In their view of flickering, the cytoskeleton can exert an active, ATP-consuming excitation of the bilayer. A similar view was shared more recently by Park et al. [10]. According to these authors, dynamic binding and unbinding of the cytoskeleton to the bilayer in the presence of ATP can increase CMF. In contrast, Evans et al. [11], and Szekely et al. [12] found a lack of ATP dependence on the CMF in the discocyte RBCs.

In this report we show that the CMF of the normal discocyte RBC, as measured with digital holographic microscopy (DHM), can be decomposed into spatially-resolved fluctuation eigenmodes. DHM and other similar quantitative phase microscopy techniques have only recently been applied to study the CMF in RBCs [10,13,14]. The instantaneous recording of the CMF on the cell surface with nanometric sensitivity along the optical axis and at high temporal and spatial resolution has several advantages over other techniques where CMF can be observed only at the rim of the cell or at single points on the cell surface. DHM is particularly well suited to explore cell dynamics [15,16] and allows for an accurate spatial analysis of the CMF [13]. We proceed the imaging data using principal component analysis (PCA) [17] to characterize the experimental CMF measurements by providing a series of spatial maps corresponding to a basis of eigenvectors that maximize the spatial variance. These experimental PCA modes are compared to deformation eigenmodes from a theoretical model of the elastic cell structure. As model parameters we include only the bending elasticity of the membrane and the stationary RBC shape that arises from bending energy minimization. However, different bending elasticity concepts have emerged over the years. Using the spontaneous curvature (SC) bending elasticity, Helfrich [18,19] was able to predict various cell shapes of the RBC that can be found in nature. The bilayer coupling hypothesis (BCH), originally introduced by Sheetz et al. [20], is a slightly different curvature concept, but leads to the same stationary RBC shapes. Peterson predicted the spatial distribution of CMF amplitudes on the RBC cell surface based on the minimization of these two bending energies [21,22]. Our model, which relies partially on the work of Peterson, allows to reproduce fluctuation eigenmodes whose spatial deformations and fluctuation amplitudes are in good agreement with the observed PCA modes. To gain a better understanding of the ATP dependency of CMF amplitudes and metabolic implications, the proposed method is applied to RBCs presenting various levels of ATP depletion. Our finding that the CMF decrease does not directly correlate with the intracellular ATP concentration during depletion questions the role of ATP as a metabolic substrate that drives CMF.

Results and Discussion

PCA mode decomposition of CMF based on DHM measurements

DHM provides instantaneous quantitative phase measurements in time and space from which the cellular thickness $d(x,t)$ can be deduced at any point on the cellular surface. CMF are assessed locally on the cell surface in a region of interest (ROI) (cf. Fig. 1D) by measuring the thickness fluctuation around the local average cell thickness. Using PCA, we are able to decompose the CMF measurements into (orthogonal) spatial maps and associated

temporally coherent fluctuations. Figure 1A shows the first 20 PCA modes X_i of a single cell remapped to the ROI and ordered by decreasing eigenvalue χ_n . The associated eigenvalue χ_n is a measure of the temporal variance of the component (see *Materials and Methods*). PCA modes can be understood as the preferential spatial deformations of the cell membrane that occur during flickering. Although PCA does not impose any spatial regularity, the obtained PCA modes show spatially well-defined patterns for the CMF of a single cell already. As can be expected for CMF that are governed mainly by the bending elasticity of the membrane, modes with large spatial wavelength exhibit the highest fluctuation amplitudes. In a control experiment the same type of measurements were obtained with paraformaldehyde fixed cells, where corresponding PCA modes showed only noisy patterns and associated eigenvalues χ_n that were about an order of magnitude lower compared to unfixed cells (cf. 1B,E). Thus the cross-linkage of proteins in the membrane with paraformaldehyde strongly inhibits CMF and no mode decomposition is detected with our approach. Using group-level PCA, the population eigenmodes for $n=198$ erythrocytes were retrieved. The inherent spatial eigenmode decomposition of CMF becomes obvious (cf. Fig. 1C). Even for a much smaller number of cells ($n \approx 20$), the same spatially well-defined PCA modes are retrieved and the first 16 components are revealed with no change in eigenvalue order. Most PCA modes have a degeneracy of two, meaning that two linearly independent PCA modes represent the same physical deformation. This property relates to the steerability of the PCA modes; e.g., the first mode can be turned along any orientation by a proper linear combination of itself and the second mode. The eigenvalues of these degenerated PCA modes are statistically equal for the group-level PCA (cf. Fig. 1E). We observed that for some single-cell recordings the eigenvalues of degenerated modes remained different, even when increasing the observation time, suggesting asymmetric shape or cell attachment that favors one (degenerate) mode versus the other. For the higher order PCA modes of the group one observes that the spatial pattern of the components is less influenced by the geometry of the cell and planar modes become predominant (see *Figure S1*).

Eigenmode decomposition based on bending deformation energy

To evaluate whether the observed PCA modes can be understood as thermally excited fluctuation eigenmodes that are, just as it is the case for the equilibrium cell shape, subject to bending energy minimization, we proceed as follows. A discocyte cell shape that minimizes the SC and BCH bending energy E_b is identified. The approach presented in Seifert et al. [23] was therefore adopted (see *Text S1*). An asymmetric cell shape that attaches to the polyornithine coated coverslip was modeled. Our hypothesis is that the regions where the cell membrane attaches to the coverslip show strongly diminished CMF and are therefore not considered as a part of the undulating membrane (see Fig. 2). CMF of the equilibrium cell shape are described by a deformation function $X(s,\phi)$ transporting the membrane in the direction normal to the cell surface. Such a deformation function can always be decomposed onto fluctuation eigenmodes $X_m(s,\phi)$ that are subject to bending energy minimization. For small deformations it is sufficient to minimize a second order energy functional in deformation coordinates (bending deformation energy) that describes the bending energy of the cell shape around its stationary configuration. We considered three different bending deformation energies, namely the SC, BCH and Laplace deformation energy (see *Materials and Methods*) and derived for each case normalized

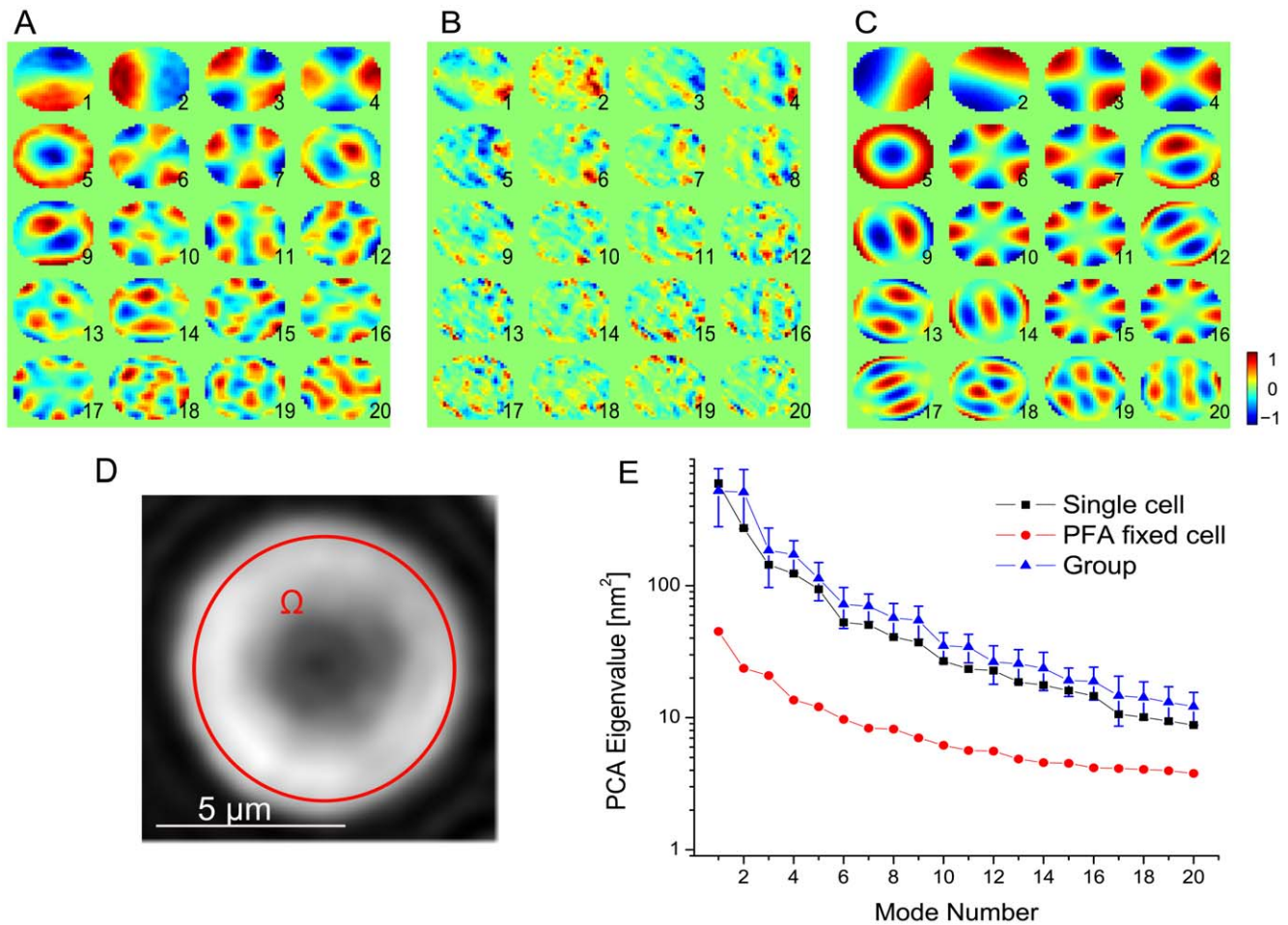


Figure 1. PCA Results. Normalized PCA modes (A) of a single cell (B) of a paraformaldehyde fixed cell (C) of a group of $n = 198$ cells. The spatial distribution of the normalized mode amplitude is color coded. (D) Phase image of erythrocyte with typical ROI for PCA analysis (E) Eigenvalues of PCA modes of A,B,C (Log Scale). Standard deviations of the values ξ_{ij} are indicated by error bars.
doi:10.1371/journal.pone.0040667.g001

energy eigenmodes $X_m(s, \phi)$ with associated bending deformation energies $\kappa \epsilon_m$.

Comparison of theoretical energy eigenmodes and experimental PCA modes

Based on the equipartition theorem which states that in thermal equilibrium each degree of freedom has an average thermal energy of $\frac{1}{2}k_b T$ (k_b Boltzmann constant, T temperature in kelvin), we can

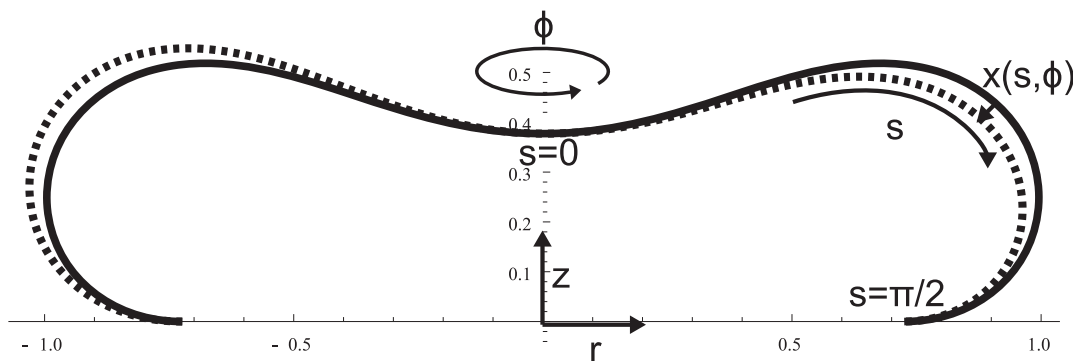


Figure 2. RBC Equilibrium Shape. Straight line: Equilibrium shape that arises from bending energy minimization (see Text S1) and which was used in the calculations to derive eigenmodes of the bending deformation energies depicted in Figure 3B,C. Dashed line: Shape of deformed cell.
doi:10.1371/journal.pone.0040667.g002

predict a mean square fluctuation amplitude $\langle u_m^2 \rangle$ for an eigenmode in a cell with radius R and bending modulus κ of

$$\langle u_m^2 \rangle = \frac{k_b TR^2}{\kappa_m}. \quad (1)$$

The validity of this approach, especially the independence of mean fluctuation amplitudes on intracellular and extracellular viscosity has been suggested by Brochard and Lennon [1]. If the equipartition theorem holds, it gives a direct link between PCA modes that maximize temporal variance of CMF data and theoretically eigenmodes that minimize the deformation energy of small deformations (see *Material and Methods* for details on how the theoretically estimated mean square fluctuation amplitude can be compared to measured PCA mode variances). In Figure 3A, a degeneracy free and separable representation of the first 9 PCA modes ordered by decreasing amplitude is shown. This representation allows comparing the PCA modes to the theoretically calculated bending deformation eigenmodes. Figures 3B and C show the theoretical eigenmodes obtained when the simple Laplace, and the BCH deformation energy, respectively, are used for the derivation. Energy eigenmodes are shown only in the ROI as they would appear in a PCA experiment. For the Laplace bending energy, the eigenmodes exhibit a spatial distribution similar to the experimental PCA modes. In addition, the amplitudes of the eigenmodes calculated with Eq. 12 and the measured amplitudes of the PCA modes are similarly distributed. Consequently, the amplitude distribution of the eigenmodes can be matched to the PCA distribution when fitting with an appropriate value of the bending modulus (cf. Fig. 3D). It follows that the mean bending modulus of the group can be determined. In order to estimate a bending modulus for individual cells, we projected each cell onto the PCA modes of the group to evaluate the mode variances ζ_{ij} . For each single cell, the bending modulus is then determined by fitting the theoretical eigenmode amplitudes to the values $\sqrt{\zeta_{ij}}$. A mean bending modulus of $\kappa = (2.75 \pm 0.78) * 10^{-19} \text{ J}$ was measured over $n = 198$ cell sample when the Laplace bending deformation energy is considered. This value is in good agreement with previous measurements in this long wavelength regime of flickering [4,24,25]. This is a surprising result considering that Laplace bending energy is usually postulated for flat, relaxed membranes. A possible physical interpretation of this result could be that the membrane can over time locally relax the bending induced strain. One could imagine a spontaneous curvature of the bilayer that is locally adapted to match the real curvature of the bilayer. Such a locally adapted spontaneous curvature would make the Laplace energy the natural description for the bending energy of small deformations. What could be a possible mechanism that would allow a relaxation of the bending energy? Bending of the bilayer, for instance towards the inner layer, is presumably accompanied with an increased lipid density on the inner layer (through compression strain) and a decreased lipid density on the outer layer (through dilation strain). Because of the fluid properties of the membrane, relaxation of compression and dilation strains in each monolayer is then likely to occur via lateral, intramembrane diffusion of lipids towards regions of lower density [26,27]. If the lipid flow is too slow to equilibrate lipid densities in the monolayers during the decay time of bending eigenmodes, then the thermally excited shape fluctuations will not be relaxed with respect to the bilayer bending energy, and a simple Laplacian term for the bending energy of small deformations might be a good approximation.

However, also eigenmode shapes and amplitudes for the BCH energy, which is a more rigorous implementation of the bending elasticity concept, are still in good agreement with the PCA results. For the SC deformation energy, the theoretical evaluation do not yield such a good match on the measures. One mode is even unstable, i.e. the evaluated energy is negative (see *Table S1 and Figure S3*). Maybe an appropriate choice of the value of C_0 could prevent this instabilities. Similar, however, to what we observe, it has already been stated in reference [24] that the BCH energy is more appropriate than the SC energy to describe CMF. Interestingly, Lim et al. [28] showed that the stomatocyte-discocyte-echinocyte shape transition can be reproduced with the BCH model upon variation of the surface area difference ΔA . Thus stationary shapes, shape transitions and CMF all support evidence for the BCH. This general validity seems to make the BCH a suitable model to describe the membrane mechanics in the RBC. However, a small discrepancy between model and experimental measurements exists. Indeed an accurate analysis of the modes in figures 3A, 3B shows similar patterns but with a minute radial scale difference. Practically, the pattern of the shown theoretical eigenmodes spreads over an area on the RBC surface slightly larger than the corresponding PCA modes restricted to the area of the ROI (see Figure S4A,B). This difference might arise from an inadequate equilibrium shape of the model. In particular, the imposed boundary constraints cannot be verified experimentally. To assess the influence of the equilibrium shape and boundary constraints, we evaluated the Laplace energy eigenmodes and associated mode amplitudes for two slightly different equilibrium shapes. A good match of the evaluated eigenmode amplitudes with the PCA mode amplitudes is preserved, while the discrepancy in spatial localization of PCA modes and theoretical eigenmodes on the cell surface is reduced, although not completely eliminated for every mode. Especially for modes with azimuthal mode number $m = 0, 2$, the discrepancy is maintained (see *Figure S5*). Additionally, the absence of a shear elasticity in the model might also contribute to this small discrepancy. In fact, Peterson [21] showed that an increased shear elasticity of the membrane tends to shift the position corresponding to maximal CMF amplitudes towards the center of the cell. When comparing measured CMF amplitude distribution on the RBC surface with the theoretical CMF amplitudes derived from the evaluated eigenmodes, we find good agreement between model and measurement, with CMF amplitudes that peak at the thickest point of the cell (see *Figure S4A,B*). Again this seems to suggest that shear elasticity of the membrane does not substantially influence CMF. The same evidence has been reported before by several authors [1,3,24,25]. Other authors, however, reported on a non-negligible influence of membrane shear elasticity on the CMF [29,30]. These different conclusions on the influence of shear elasticity on flickering presumably originate from the different theoretical models that are used to fit the elastic moduli. With regard to the applied theoretical models, we consider it important that models take into account the equilibrium shape, as the measured PCA modes show how strong CMF are influenced by the equilibrium shape of the RBC.

The investigated PCA modes and inferred bending modulus describe the membrane fluctuations in a long wavelength regime. In a short wavelength regime, however, a bending modulus approximately ten fold lower has been measured [1–3]. Indeed, when the mean square fluctuation amplitudes $\langle u_q^2 \rangle$ of planar modes are expressed in terms of spatial wave vector $|q|$, we observe, in a short wavelength regime, an eightfold increase of the fluctuation amplitudes when compared to the theoretically expected amplitudes for pure bending modes calculated with a bending modulus value κ measured in the long wavelength regime

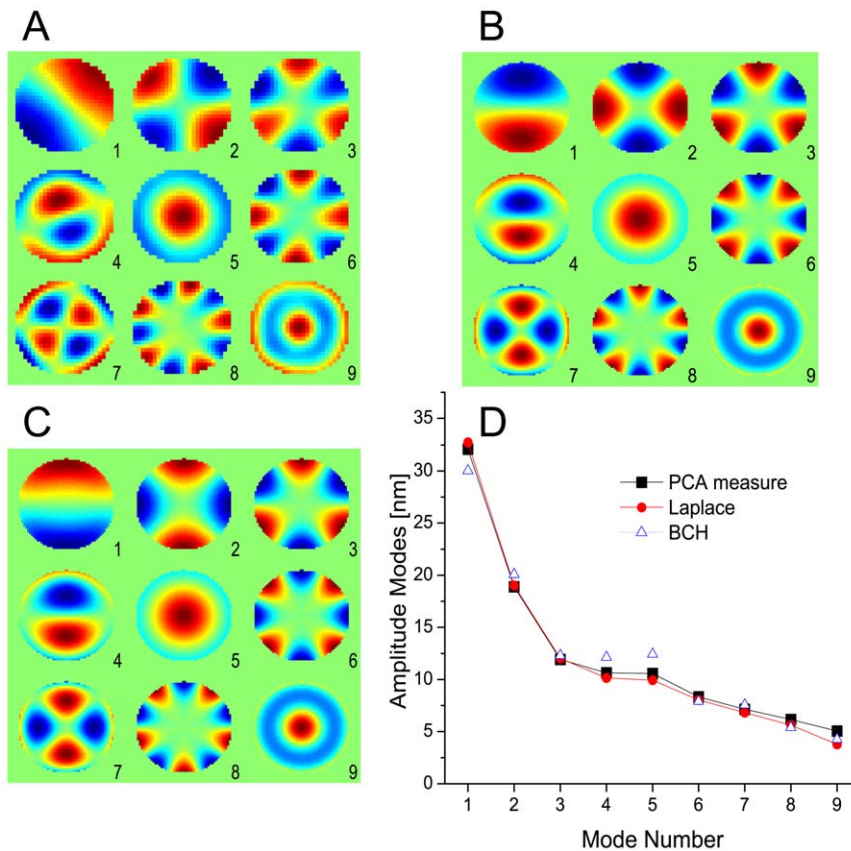


Figure 3. Experimental and Theoretical Comparison. (A) Degeneracy free representation of PCA modes. The separable modes 7 (degeneracy of 2) and 9 in this representation are obtained from an appropriate linear combination of the degenerate modes 12,13 and 14 of Figure 1C. Both representations are equivalent, because they span the same subspace. (B) Eigenmodes that minimize Laplace deformation energy shown in the ROI. Eigenmodes are plotted as functions $X_m(r,\phi)$ (C) Eigenmodes that minimize BCH Deformation Energy shown only in the ROI (D) Comparison of theoretical and measured fluctuation amplitudes. doi:10.1371/journal.pone.0040667.g003

(see Figure S2). It has been argued that this higher apparent bending modulus of the long wavelength regime compared to the short wavelength one, can be attributed to fluctuations of coupled fluid and solid membranes, i.e. bilayer and cytoskeleton [6]. A similar result has been reported recently by Park et al. [29] who measure a low bending stiffness also in the long wavelength regime, but include shear and area compressibility modulus to accommodate measurements and applied theoretical model. Thus the higher apparent bending modulus in the long wavelength regime would not only comprehend the bending modulus of the bilayer, but include terms related to the cytoskeleton and its interaction with the bilayer. If so, it is then surprising that the measured PCA modes can be properly described by a pure bending deformation energy model, which neglects the shear modulus of the cytoskeleton.

CMF in ATP depleted RBCs

Bending energy eigenmodes whose amplitudes can be predicted based on the equipartition theorem seem to be in contradiction with active ATP-consuming mechanisms. Therefore, we applied the PCA method to investigate CMF in RBCs with various levels of ATP depletion. After 1 hour of incubation in the depletion medium, the equilibrium shape of all the RBCs in the population still remained biconcave. After 2 h of incubation the onset of echinocyte formation with small spicule protrusions on the cell rim was observed in some cells of the population, whereas after 4 h of

incubation nearly all cells were spiculated. Fig. 4A shows the respective mean fluctuation amplitudes of the first 6 bending modes depicted in Fig. 3A. To assess the dynamics of the ATP depletion protocol, intracellular ATP levels were measured via luciferase chemiluminescence, whose emitted intensity is proportional to ATP concentration [31] (cf. Fig. 4B). A significant fluctuation amplitude decrease after 4 h of ATP depletion is observed for every PCA mode in a population of $n=36$ cells. Interestingly, after 4 h a subpopulation of cells did not show any spatially coherent fluctuations, i.e. the single cell PCA modes were not spatially well-defined and also the temporal variances ξ_{ij} of the group PCA mode projections were nearly zero. Alteration of the membrane mechanical properties resulting from a strong binding of the cytoskeleton to the bilayer and/or a rigidification of the cytoskeleton could adequately explain such a result. Often such an increase in membrane rigidity upon ATP depletion is attributed to the dephosphorylation of the skeletal protein 4.1R that causes a reinforced binding to the transmembrane protein Glycophorin C and the actin filament at the junction of the spectrin tetramer in the cytoskeleton [10,32,33]. A further ATP dependent factor that might impact on CMF is the maintenance of lipid asymmetry in the bilayer via ATP consuming translocase activity (flippases and floppases). The phospholipid distribution among the leaflets has been shown to modulate RBC membrane elasticity through altered spectrin-lipid interactions [34]. A possible mechanism is for instance the glycation of membrane-associated spectrin after

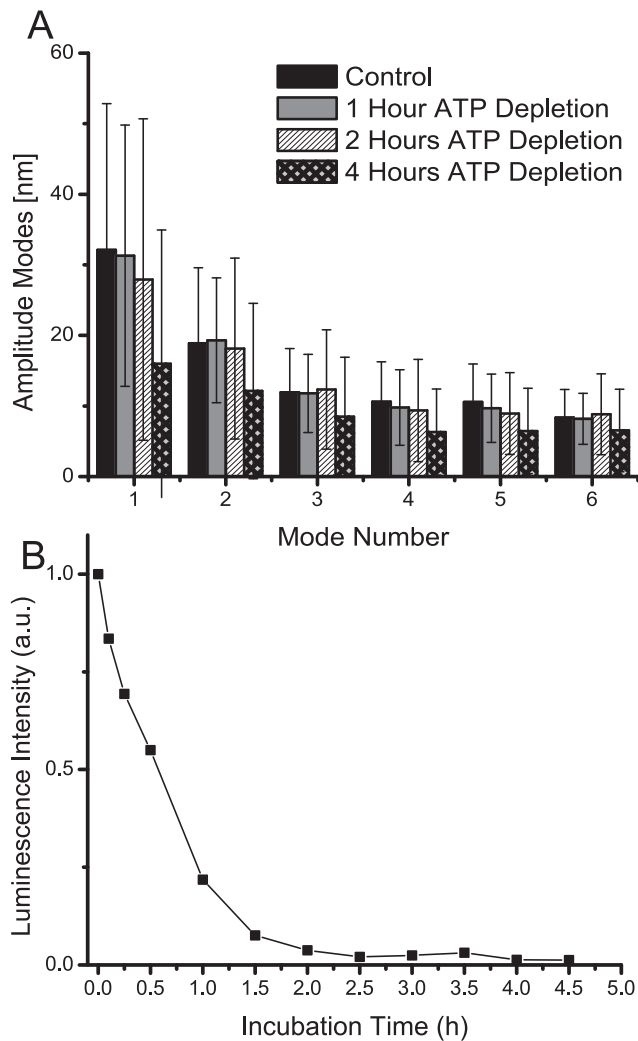


Figure 4. ATP Depletion in RBC. (A) Fluctuation amplitudes of the first six PCA modes in a population of $n=198$ (no ATP depletion), 43 (1 h ATP depletion), 47 (2 h ATP depletion), 36 (4 h ATP depletion) cells. (B) Assessment of intracellular ATP level at different instants of incubation time in depletion medium through the measurement of chemiluminescence intensity of luciferin luciferase assay in RBC cell solution.

doi:10.1371/journal.pone.0040667.g004

disruption of lipid asymmetry through ATP depletion, which has been shown to reduce membrane deformability [35].

In contrast, an ATP-powered mechanism that would transfer mechanical energy to the bilayer and act as driving force of CMF as has been proposed by several authors [8–10,33] should lead to fluctuation amplitudes that correlate with the intracellular ATP concentration. However, after 1 h of incubation in the depletion medium, where there are no significant changes of RBC cell shape or mode fluctuation amplitudes, the intracellular ATP concentration is reduced to $\approx 20\%$ of the initial level. If ATP supplies energy to drive CMF, a drastic decrease in ATP should be reflected in decreased CMF. The observation that the intracellular ATP concentration is not correlated to CMF amplitudes and RBC shape has also been stated more recently by Szekely et al. [12]. As ATP plays certainly an important role in the maintenance of the mechanical properties of the composite membrane, our results suggests that ATP does not act as an active driving force of CMF.

An additional argument is that the mean fluctuation amplitudes of the eigenmodes respect thermal equilibrium theory. However, this is not a definitive proof of the thermal origin of CMF, since it has been assumed that it is valid to model the effects of ATP by an increased effective temperature and preserve in this way thermal equilibrium [9]. However, one would expect in such a case a direct relation between CMF amplitudes and intracellular ATP concentration. In our view, the decrease of CMF after complete ATP depletion arises from the changed mechanical properties of the bilayer-cytoskeleton complex. The chemical processes that cause these mechanical changes are not yet fully understood. Similar to what has been suggested for ATP-mediated cell shape changes [36,37], it seems that intracellular ATP does not directly determine CMF, but is among other factors responsible for the maintenance of the biomechanical properties of the cellular membrane.

Conclusion

We have shown that the PCA which decomposes the experimental CMF measurements based only on a variance maximization criterium allows to identify spatially well-defined modes over the RBC surface. These PCA modes were confronted with a theoretical eigenmode decomposition of CMF which results from a quantization of the membrane deformation energy for fluctuations constrained by boundary conditions. Practically, considering only the bending deformation energy of the cell membrane around its stationary configuration has permitted to obtain eigenmodes presenting spatial patterns in good agreement with the PCA modes. In addition, the amplitude distribution of the eigenmodes calculated according to the equipartition theorem is similar to the amplitude distribution of the measured PCA modes. Consequently, matching the eigenmode amplitude distribution to the PCA amplitude distribution has allowed to determine the value of bending modulus κ . Experiments aimed at exploring the role played by ATP seem to favor a view in which CMF of erythrocytes are the result of thermal agitation governed mainly by the bending resistance of the cell membrane, whose mechanical properties are maintained by the presence of the intracellular ATP. Our approach which allows to characterize the CMF represents a useful tool to detect subtle changes in the mechanical properties of the RBC membrane.

Materials and Methods

Ethics statement

Blood withdrawal from healthy laboratory personnel was ethically approved by the Commission cantonale (VD) de la recherche sur l'être humain, Sous-Commission III, Rue César-Roux 19, 1005 Lausanne on January 16th 2012.

Cell preparation

100–150 μl of blood was drawn by fingerpick, collected and diluted at a ratio of 1:10 (v/v) in cold HEP buffer (15 mM HEPES pH 7.4, NaCl 130 mM, KCl 5.4 mM and 10 mM glucose). Blood cells were sedimented at 200 g, 4°C for 10 min and buffy coat was gently removed. RBCs were washed twice in HEP buffer (1000 $g \times 2$ min at 4°C). Finally, erythrocytes were suspended in HEPA buffer (15 mM HEPES pH 7.4, 130 mM NaCl, 5.4 mM KCl, 10 mM glucose, 1 mM CaCl₂, 0.5 mM MgCl₂ and 1 mg/ml bovine serum albumin) at 0.2% hematocrit. 4 μl of the erythrocyte suspension were diluted to 150 μl of HEPA buffer and introduced into the experimental chamber, consisting of two cover slips separated by spacers 1.2 mm thick. The bottom coverslip was coated with polyornithine to ensure that cells adhere to the coverslip surface. This suppresses translational movements of the

cells during acquisition and diminishes CMF of the attached cell membrane. Cells were incubated for 30 min at a temperature of 37°C before mounting the chamber on the DHM stage. All experiments were conducted at room temperature (22°C) and only cells displaying a normal discocyte shape were selected for analysis. All the experimental work reported in this paper relied only on blood samples taken from the co-authors DB and AH.

Irreversible ATP depletion in RBCs. RBCs were diluted in a glucose free HEPA buffer containing inosine, which consumes ATP, and iodoacetamide, that inhibits glycolysis. (10 mM HEPES, 120 mM NaCl, 5.4 mM KCl, 1.8 mM CaCl₂, 0.8 mM MgCl₂, 0.9 mM NaH₂P0₄, 6 mM iodoacetamide, 10 mM inosine, 1 mg/ml bovine serum albumin) CMF measurements were conducted at room temperature after 1 h, 2 h and 4 h of incubation at 37°C.

Measurement of ATP levels during depletion. Intracellular ATP content was assessed via the chemiluminescence intensity of a luciferin-luciferase based assay kit purchased from Promega (CellTiter-Glo Luminescence Cell Viability Assay). Luminescence intensity measurements were performed on a Tecan Safire well plate reader.

DHM

Holograms were acquired on a transmission DHM setup (DHM T1000TM, LyncéeTec SA, Lausanne, Switzerland) as described in [15]. Briefly, the experimental setup is a modified Mach-Zehnder configuration with a laser diode source ($\lambda = 683$ nm). The laser beam is split into a reference wave R and an object wave O. The latter is diffracted by the specimen, magnified by a 40X/0.75 NA microscope objective and interferes, in an off-axis geometry, with the reference wave to produce the hologram intensity recorded by the CCD camera. The reconstruction of the object wavefront is achieved through a numerical re-illumination of the hologram by a digital computed reference wave. The algorithm used for the wavefront reconstruction and aberration compensation has been described in [38]. Along the optical axis a nanometric sensitivity in cell height variations is achieved; laterally DHM shows a diffraction limited resolution. Holograms of 256×256 pixels are acquired at a rate of 25 Hz from which phase images are reconstructed with custom-made software from LyncéeTec SA.

PCA decomposition of CMF

As a first pre-processing step to PCA, the measured phase shift $\varphi(\chi, \tau)$ is converted into cellular thickness. Under the assumption of a constant cellular index of refraction this relation is given by

$$d(x, t) = \frac{\lambda}{2\pi(n_{cell} - n_{sol})} \varphi(\chi, \tau) \quad (2)$$

A mean cellular refractive index of 1.394, calculated by the same microscopic technique [39] and a refractive index of the HEPA solution of 1.3334 was therefore used. The assumption of a constant intracellular refractive index within the RBC volume is motivated by the fact that in the human RBC, lacking intracellular organelles and nucleus, the high refractive index is primarily due to the hemoglobin content that we suppose equally distributed within the cell. As a further preprocessing step, RBC images were aligned with an image registration algorithm [40] to ensure that local thickness variations were not due to a translational movement of the cell. A region of interest (ROI) (cf. Fig. 1D) is defined on the RBC that stretches slightly beyond the position of maximal thickness, but excludes the borders of the erythrocyte, since in these regions the cell surface shows high inclination with respect to the x-y plane (cf. Fig. 1D and Figure S4). These inclined border regions are not included because a small horizontal movement of the membrane translates into a strong axial

displacement. The local thickness fluctuation amplitude $u(x, t)$ for each pixel contained in the ROI is obtained by subtracting the temporal mean from the current thickness.

$$u(x, t) = d(x, t) - \langle d(x, t) \rangle_t \quad (3)$$

Because of the attachment of the lower RBC surface to the coverslip, we interpret the measured thickness fluctuations essentially as CMF of the upper (concave) RBC surface. PCA provides an orthogonal linear transformation that maps input data such that subsequent components maximize variance. PCA was applied to the spatial dimension of RBC fluctuations. Fluctuation amplitudes are stored in a matrix U,

$$U = \begin{pmatrix} u(x_1, t_1) & \cdots & u(x_1, t_l) \\ \vdots & \ddots & \vdots \\ u(x_n, t_1) & \cdots & u(x_n, t_l) \end{pmatrix} \quad (4)$$

where $l = 1000$ images acquired over 40 s of a single cell region containing n pixels serve as input for the matrix U. By diagonalizing the covariance matrix $C_x = (U \cdot U^T)$, a spatial decomposition of the RBC membrane fluctuations that maximizes the variance (eigenvalue) χ_i of the PCA mode (eigenvector) X_i while cancelling out the covariance between modes is obtained. PCA modes X_i were ordered according to the importance of the associated variance χ_i .

Group PCA analysis. The method presented in the preceding paragraph restricts the analysis to a single cell. It is, however, important to extend the method to a larger number of cells and find the preferential PCA modes of a population. Therefore, RBC phase images are first reinterpolated to match the contour of a circular model cell. Resizing is performed with cubic spline interpolation. Artifacts of the interpolation procedure are estimated to be negligible, as PCA analysis results (eigenvalues and eigenmodes) on a single cell level are not altered by the cubic spline interpolation. The spatial covariance matrix of the group is obtained by summing up the covariance matrices of each cell,

$$C_x = \sum_{j=0}^n (U_j \cdot U_j^T) / l_j, \quad (5)$$

where n denotes the number of cells in the group and l_j the number of acquired images of cell j . Diagonalization leads then again to the PCA modes. To assess the temporal evolution of a mode X_i for a cell j we project the matrix U_j onto X_i to form a vector u_{ij} that holds the time course of the mode. The squared norm ξ_{ij} of this vector, i.e. the temporal variance of the mode projection, can be compared to the eigenvalue χ_i to evaluate the contribution of the cell to the PCA mode.

Determination of bending deformation energy eigenmodes

An eigenmode that transports the membrane in a direction normal to the cell surface at each point (s, ϕ) of the undulating membrane is described by a separable ansatz $X_m(s, \phi) = f(s) \cos(m * \phi)$, with m denoting the azimuthal number (cf. Fig. 2). In-plane-motions are not considered in the model because shape preserving displacements of the membrane do not alter bending energies. To determine the energy of a theoretical eigenmode X_m one can expand the bending energy E_b about its minimum up to second order with respect to a normal motion X_m . The first order term vanishes by stationarity and the second order

term, the bending deformation energy, is a quadratic form in deformation coordinates as follows

$$E_b(X_m) = E_b(0) + \frac{\kappa}{2} \langle X_m | \delta^2 E_b | X_m \rangle. \quad (6)$$

In this definition, the expression $\delta^2 E_b$ is a unitless measure of the energy cost of a deformation X_m depending entirely on the cell geometry. In the case of the SC and BCH bending energies, Peterson [21,22] derived explicit expressions for the bending deformation energy $\frac{\kappa}{2} \delta^2 E_b$ of normal motions X_m . Further, another quadratic form referenced as Laplace deformation energy was investigated:

$$\langle X | \delta^2 E_b | X \rangle_{Laplace} = \int_M (\Delta X)^2 dA. \quad (7)$$

The Laplace deformation energy corresponds to the second order bending energy expansion for a flat, infinite, membrane. As such it must be considered as an ad-hoc approach when describing the bending deformation energy of a closed RBC cell shape.

To find an energy eigenmode $X_m(s, \phi)$ that minimizes the quadratic bending deformation energy $\kappa \epsilon_m$, the Ritz method is applied. Following the Ritz method, we express the energy eigenmode $X_m(s, \phi)$ that minimizes a quadratic energy functional as a linear combination of basis functions $X_m(s, \phi) = \sum_i^N c_{im} \Psi_i(s, \phi)$ that all meet imposed constraints. In the present case, these constraints are $\Psi_i(\frac{\pi}{2}, \phi) = \frac{\partial \Psi_i}{\partial s}(\frac{\pi}{2}, \phi) = 0$, i.e. the deformation function and its derivative vanish where the cell attaches to the coverslip. Additionally, for modes with azimuthal number $m=0$, one must take care that the cell does not change its initial volume in a deformation. Linear combinations of sinusoidal functions that respect the constraints are found as a convenient basis of functions $\Psi_i(s, \phi)$. The deformation energy of an eigenmode with a normalized amplitude on the undulating membrane M with surface area A_M is then given by

$$\epsilon = A_M \frac{\langle \sum_i c_i \Psi_i | \delta^2 E_b | \sum_i c_i \Psi_i \rangle}{\langle \sum_i c_i \Psi_i | \sum_i c_i \Psi_i \rangle} = A_M \frac{\sum_i \sum_j c_i c_j H_{ij}}{\sum_i \sum_j c_i c_j S_{ij}} \quad (8)$$

For instance, the element H_{ij} for the Laplace deformation energy writes in local coordinates (s, ϕ) as

$$H_{ij} = \int_M (\Delta \Psi_i \Delta \Psi_j) dA_M = \int_M \left(\frac{\partial^2 \Psi_i}{\partial s^2} + 1/r \frac{\partial \Psi_i}{\partial s} \frac{\partial r}{\partial s} + 1/r^2 \frac{\partial^2 \Psi_i}{\partial \phi^2} \right) \left(\frac{\partial^2 \Psi_j}{\partial s^2} + 1/r \frac{\partial \Psi_j}{\partial s} \frac{\partial r}{\partial s} + 1/r^2 \frac{\partial^2 \Psi_j}{\partial \phi^2} \right) r d\phi ds. \quad (9)$$

One must evaluate the matrix H for each azimuthal number m , the indice was omitted for simplicity. The vector C of basis function coefficients c_i for the eigenmode and the minimized deformation energy ϵ are then found by solving the eigenvalue problem $A_M S^{-1} H C = \epsilon C$. Eigenmodes with the lowest (or second lowest) eigenvalues are considered in each azimuthal number class when comparing with the measured PCA modes.

Comparison of theoretical mean square fluctuation amplitude and PCA mode variances

An amplitude u of a deformation function $X(s, \phi)$ on the undulating membrane M is evaluated as

$$u = \sqrt{\int_M [X(s, \phi)^2] dA / A_M}, \quad (10)$$

where A_M is the surface of the undulating membrane. Bending deformation energies ϵ_m are evaluated for energy eigenmodes $X_m(s, \phi)$ normalized in the sense of Eq. [10]. Similarly, experimental PCA modes X_i are normalized with respect to the surface area of the ROI A_{ROI} (cf. Fig. 1D). Because DHM cannot assess the CMF on the whole fluctuating membrane surface, but only in a restricted ROI, one must introduce a correction factor when relating the theoretically calculated mean square fluctuation amplitudes $\langle u_m^2 \rangle$ to the measured PCA mode variances χ_i . This factor for an eigenmode X_m is given by

$$f_m = \frac{\int_{ROI} X_m(s, \phi)^2 dA / A_{ROI}}{\int_M X_m(s, \phi)^2 dA / A} \quad (11)$$

such that the theoretically expected variance as captured by a PCA mode is

$$\langle u_m^2 \rangle_{PCA} = f_m \cdot \langle u_m^2 \rangle = \frac{k_b T R^2}{\kappa \tilde{\epsilon}_m}. \quad (12)$$

Supporting Information

Text S1 Bending elasticity and equilibrium shape.

(PDF)

Table S1 Bending deformation energies $\tilde{\epsilon}_m$ for eigenmodes depicted in Figures 3 and S3. The evaluated values $\tilde{\epsilon}_m$ used for the estimation of the expected PCA mode variances in equation 10 are shown in the the Table S1.

(PDF)

Figure S1 Higher order PCA modes from the discocyte RBC group of $n = 198$ cells.

For the higher order (lower energy) PCA modes one observes that the spatial pattern of the components is less influenced by the geometry of the cell as the PCA mode variance decreases. Planar waves seem therefore to be a good decomposition basis of the membrane fluctuations for spatial frequencies $q > 2\pi \frac{2}{R_{cell}} \approx 0.0027$ rad/nm.

(EPS)

Figure S2 ATP depletion/Decomposition of membrane fluctuation onto planar modes.

(A) Mean fluctuation amplitudes $\langle \sqrt{u(t)^2} \rangle_t$ of individual cells averaged in the ROI after $t = 0, 1, 2, 4$ h of incubation in depletion medium for $n = 198, 43, 47, 36$ cells. After 4 hours of ATP depletion, about half of the cells showed clearly reduced fluctuation amplitudes. These cells showed strongly reduced coherent fluctuations in the PCA approach. (B) Mean square fluctuation amplitudes of planar modes $\langle u_q^2 \rangle_t$ in function of spatial wavevector $|q|$, $n = 198$ cells, error bars denote SD-Value. Measured mean square fluctuation amplitudes $\langle u_q^2 \rangle$ were normalized by theoretically expected amplitudes of bending modes $\langle u_q \rangle_b^2 = \frac{k_b T}{\kappa S q^4}$. The value

for the bending modulus $\kappa = 2.75e^{-19} J$ was measured based on PCA modes in the long wavelength regime. Independently of intracellular ATP concentration, an increase of fluctuation amplitudes with respect to pure bending modes are observed for spatial wavevectors $q > 0.003$ rad/nm. For fluctuations at high spatial frequencies, the standard deviation around the measured average fluctuation amplitudes

($n = 198$ cells) increases considerably. This can partially be explained by experimental noise: DHM and other quantitative phase imaging methods are confronted with noise at higher spatial frequencies that also contributes to the measured mean square fluctuation amplitudes at high spatial wavevectors. Therefore, we think that the measurements must be taken with precaution for $q > 0.005$.

(EPS)

Figure S3 Spontaneous curvature (SC) bending deformation eigenmodes.

(EPS)

Figure S4 Experimental and theoretical CMF amplitude distribution on RBC surface/Visualisation of ROI used for PCA and theoretical model. (A) Mean CMF amplitudes

$\sqrt{\langle u(x,t)^2 \rangle_t}$ measured in a group of $n = 198$ cells (green line) along average profile of RBC surface (blue line). The measured amplitudes have been corrected by a factor $\cos(\theta)$, where θ is the angle that the surface normal makes with the z-axis. Black vertical lines indicate the boundaries of the ROI that was used for PCA analysis. (B) Equilibrium shape of model cell 1 (straight line) and theoretical CMF amplitude distribution (dashed line) obtained by adding the mean squared fluctuation amplitudes of the first 9 eigenmodes depicted in Figure 3B. Amplitude is overestimated for better visibility. Black vertical lines indicate the boundaries of the theoretical eigenmodes depicted in Figure 3B,C. (C) Theoretical CMF amplitudes (green line) along profile of RBC equilibrium shape (blue line). Amplitudes have been corrected by a factor $\cos(\theta)$. This representation of the theoretical results is in good agreement with experimental data in (A).

(EPS)

References

- Brochard F, Lennon JF (1975) Frequency spectrum of the flicker phenomenon in erythrocytes. *J Phys France* 36: 1035–1047.
- Zilker A, Engelhardt H, Sackmann E (1987) Dynamic reflection interference contrast (ric-) microscopy - a new method to study surface excitations of cells and to measure membrane bending elastic-moduli. *Journal De Physique* 48: 2139–2151.
- Zilker A, Ziegler M, Sackmann E (1992) Spectral analysis of erythrocyte flickering in the 0.3–4 μm^{-1} regime by microinterferometry combined with fast image processing. *Physical Review A* 46: 7998.
- Strey H, Peterson M, Sackmann E (1995) Measurement of erythrocyte membrane elasticity by flicker eigenmode decomposition 69: 478–488.
- Gov N, Zilman AG, Safran S (2003) Cytoskeleton confinement and tension of red blood cell membranes. *Physical Review Letters* 90: 228101.
- Auth T, Safran SA, Gov NS (2007) Fluctuations of coupled fluid and solid membranes with application to red blood cells. *Physical Review E* 76: 051910.
- Levin S, Korenstein R (1991) Membrane fluctuations in erythrocytes are linked to mgatp-dependent dynamic assembly of the membrane skeleton. *Biophysical Journal* 60: 733–737.
- Tuvia S, Levin S, Bitler A, Korenstein R (1998) Mechanical fluctuations of the membrane-skeleton are dependent on f-actin atpase in human erythrocytes. *Journal of Cell Biology* 141: 1551–1561.
- Gov NS, Safran SA (2005) Red blood cell membrane fluctuations and shape controlled by atp-induced cytoskeletal defects (vol 88, pg 1859, 2005). *Biophysical Journal* 89.
- Park Y, Best CA, Auth T, Gov NS, Safran SA, et al. (2010) Metabolic remodeling of the human red blood cell membrane. *Proc Natl Acad Sci U S A*.
- Evans J, Gratzler W, Mohandas N, Parker K, Sleep J (2008) Fluctuations of the red blood cell membrane: Relation to mechanical properties and lack of atp dependence. *Biophysical Journal* 94: 4134–4144.
- Szekely D, Yau T, Kuchel P (2009) Human erythrocyte flickering: temperature, atp concentration, water transport, and cell aging, plus a computer simulation. *European Biophysics Journal* 38: 923–939.
- Rappaz B, Barbul A, Hoffmann A, Boss D, Korenstein R, et al. (2009) Spatial analysis of erythrocyte membrane fluctuations by digital holographic microscopy. *Blood Cells Molecules and Diseases* 42: 228–232.
- Popescu G, Ikeda T, Goda K, Best-Popescu CA, Laposata M, et al. (2006) Optical measurement of cell membrane tension. *Physical Review Letters* 97: 218101–4.
- Marquet P, Rappaz B, Magistretti PJ, Cuhe E, Emery Y, et al. (2005) Digital holographic microscopy: a noninvasive contrast imaging technique allowing quantitative visualization of living cells with subwavelength axial accuracy. *Opt Lett* 30: 468–470.
- Jourdain P, Pavillon N, Moratal C, Boss D, Rappaz B, et al. (2011) Determination of transmembrane water fluxes in neurons elicited by glutamate ionotropic receptors and by the cotransporters kcc2 and nkcc1: A digital holographic microscopy study. *The Journal of Neuroscience* 31: 11846–11854.
- Jolliffe I (2002) *Principal Component Analysis*. Springer Series in Statistics, second edition.
- Helfrich W (1973) Elastic properties of lipid bilayers: theory and possible experiments. *Z Naturforsch C* 28: 693–703.
- Deuling H, Helfrich W (1976) The curvature elasticity of fluid membranes: A catalogue of vesicle shapes. *J Phys France* 37: 1335–1345.
- Sheetz MP, Singer SJ (1974) Biological membranes as bilayer couples. a molecular mechanism of drug-erythrocyte interactions. *Proceedings of the National Academy of Sciences of the United States of America* 71: 4457–4461.
- Peterson MA (1992) Linear response of the human erythrocyte to mechanical stress. *Physical Review A* 45: 4116.
- Peterson MA (1985) Geometrical methods for the elasticity theory of membranes. *Journal of Mathematical Physics* 26: 711–717.
- Seifert U, Berndl K, Lipowsky R (1991) Shape transformations of vesicles: Phase diagram for spontaneous- curvature and bilayer-coupling models. *Physical Review A* 44: 1182.
- Mark AP, Helmut S, Erich S (1992) Theoretical and phase contrast microscopic eigenmode analysis of erythrocyte flicker: amplitudes. *J Phys II France* 2: 1273–1285.
- Zeman K, Engelhard H, Sackmann E (1990) Bending undulations and elasticity of the erythrocyte membrane: effects of cell shape and membrane organization. *Eur Biophys J* 18: 203–19.
- Fischer TM (1992) Bending stiffness of lipid bilayers. i. bilayer couple or single-layer bending? *Biophysical Journal* 63: 1328–1335.
- Seifert U, Langer SA (1993) Viscous modes of fluid bilayer membranes. *Europhysics Letters* 23: 71.
- Lim HWG, Wortis M, Mukhopadhyay R (2002) Stomatocytoid erythrocyte sequence of the human red blood cell: Evidence for the bilayer couple hypothesis from membrane mechanics. *Proceedings of the National Academy of Sciences of the United States of America* 99: 16766–16769.

Figure S5 Influence of equilibrium shape and boundary conditions on Laplace deformation energy eigenmodes.

(A) Equilibrium shape of model cell 2 (straight line) and theoretical CMF amplitude distribution (dashed line) obtained by adding the mean squared fluctuation amplitudes of the first 9 eigenmodes depicted in Figure S5C. CMF Amplitude is overestimated for better visibility. Black vertical lines indicate the boundaries of the theoretical eigenmodes depicted in Figure S5C (B) Equilibrium shape of model cell 3 (straight line) and theoretical CMF amplitude distribution (dashed line) obtained by adding the mean squared fluctuation amplitudes of the first 9 eigenmodes depicted in Figure S5D. Black vertical lines indicate the boundaries of the theoretical eigenmodes depicted in Figure S5D. (C) Eigenmodes that minimize Laplace deformation energy shown in the ROI for model cell 2. Eigenmodes are plotted as functions $X_m(r,\phi)$ (D) Eigenmodes that minimize Laplace deformation energy shown in the ROI for model cell 3. (C) Comparison of theoretical and measured fluctuation amplitudes of PCA modes.

(EPS)

Acknowledgments

We would like to thank the collaborators of LyncéeTec for technical assistance and Prof. Erich Sackmann and Dr. Sandor Kasas for helpful discussions.

Author Contributions

Conceived and designed the experiments: DB BR PJM DVD PM. Performed the experiments: DB AH. Analyzed the data: DB AH. Contributed reagents/materials/analysis tools: CD DVD. Wrote the paper: DB PM DVD PJM. Designed the software used in analysis: DB BR DVD.

29. Park Y, Best CA, Badizadegan K, Dasari RR, Feld MS, et al. (2010) Measurement of red blood cell mechanics during morphological changes. *Proceedings of the National Academy of Sciences* 107: 6731–6736.
30. Hale JP, Marcelli G, Parker KH, Winlove CP, Petrov PG (2009) Red blood cell thermal fluctuations: comparison between experiment and molecular dynamics simulations. *Soft Matter* 5: 3603–3606.
31. Mikirova N, Riordan H, Kirby K, Klykov A, Jackson J (2005) Monitoring of atp levels in red blood cells and t cells of healthy and ill subjects and the effects of age on mitochondrial potential. *Orthomolecular Medicine* 20(1): 50–58.
32. Manno S, Takakuwa Y, Mohandas N (2005) Modulation of erythrocyte membrane mechanical function by protein 4.1 phosphorylation. *Journal of Biological Chemistry* 280: 7581–7587.
33. Betz T, Lenz M, Joanny JF, Sykes C (2009) Atp-dependent mechanics of red blood cells. *Proceedings of the National Academy of Sciences* 106: 15320–15325.
34. Manno S, Takakuwa Y, Mohandas N (2002) Identification of a functional role for lipid asymmetry in biological membranes: Phosphatidylserine-skeletal protein interactions modulate membrane stability. *Proceedings of the National Academy of Sciences* 99: 1943–1948.
35. Manno S, Mohandas N, Takakuwa Y (2010) Atp-dependent mechanism protects spectrin against glycation in human erythrocytes. *Journal of Biological Chemistry* 285: 33923–33929.
36. Sheetz MP, Singer SJ (1977) On the mechanism of atp-induced shape changes in human erythrocyte membranes. i. the role of the spectrin complex. *The Journal of Cell Biology* 73: 638–646.
37. Feo C, Mohandas N (1977) Clarification of role of atp in red-cell morphology and function. *Nature* 265: 166–168.
38. Colomb T, Montfort F, Khn J, Aspert N, Cuche E, et al. (2006) Numerical parametric lens for shifting, magnification, and complete aberration compensation in digital holographic microscopy. *J Opt Soc Am A* 23: 3177–3190.
39. Rappaz B, Barbul A, Emery Y, Korenstein R, Depeursinge C, et al. (2008) Comparative study of human erythrocytes by digital holographic microscopy, confocal microscopy, and impedance volume analyzer. *Cytometry Part A* 73A: 895–903.
40. Thevenaz P, Ruttimann UE, Unser M (1998) A pyramid approach to subpixel registration based on intensity. *Ieee Transactions on Image Processing* 7: 27–41.